Electronic structure and magnetic and transport properties of single-crystalline UN

M. Samsel-Czekała,[1] E. Talik,[2] P. de V. Du Plessis,[3] R. Troć,[1] H. Misiorek,[1] and C. Sułkowski[1]
[1]*Institute of Low Temperature and Structure Research, Polish Academy of Sciences, P.O. Box 1410, 50-950 Wrocław 2, Poland*
[2]*Institute of Physics, University of Silesia, Uniwersytecka 4, 40-007 Katowice, Poland*
[3]*Physics Department, University of Johannesburg, P.O. Box 524, Aucklandpark 2006, Johannesburg, South Africa*
(Received 22 June 2007; revised manuscript received 5 September 2007; published 22 October 2007)

The electronic structure (both valence band and 4*f* core level spectra) of the cubic monocompound UN in the paramagnetic state was studied by x-ray photoelectron spectroscopy. The experimental results are compared with the results of calculations employing full-potential local-orbital minimum-basis full relativistic method with the spin-orbit coupling included implicitly. The molar susceptibility of a single crystal of antiferromagnetic UN (T_N=51 K) is reported along three main crystallographic directions between 1.9 and 300 K. The observed magnetic characteristics are in agreement with previous studies. The observed small anisotropy in the ordered region is discussed. Results of electronic structure, magnetoresistivity, thermoelectric power, and thermal conductivity as studied on single-crystalline specimens are given and discussed from the viewpoint of dual and spin-density-wave-like character of the 5*f* electrons.

DOI: 10.1103/PhysRevB.76.144426 PACS number(s): 75.30.Fv, 71.20.−b, 72.15.Eb, 75.47.−m

I. INTRODUCTION

Up to now, a very large number of experimental studies have been reported on the magnetic, thermal, and electrical properties of uranium mononitride (UN) polycrystalline samples. References to older and recent research, as well as summaries of these results, have recently been collected in a comprehensive tabulation of data in Landolt-Börnstein.[1] Also in the past, many studies on single crystals of UN were performed, viz., susceptibility $\chi(T)$,[2] resistivity $\rho(T)$,[3,4] elastic constants,[5–7] x-ray diffraction,[8,9] elastic[10–12] and inelastic[13,14] neutron scattering, and photoemission[15–17] experiments. Nevertheless, many outstanding aspects of its behavior are still to be explained.

UN has a fcc crystal structure in its paramagnetic (PM) region and orders[10] in a type I antiferromagnetic (AFM) structure with spins aligned along the [100] axis below its Néel temperature $T_N \cong 53$ K. The expected tetragonal distortion associated with AFM order of this type turned out to be very small ($|c/a-1|=6.5\times10^{-4}$ at 4.2 K)[8] and its existence or nonexistence has even been a subject of some controversy.[9] A single crystal of UN in its AFM state is expected to have an equal population of magnetic domains associated with the [100], [010], and [001] directions. Rossat-Mignod *et al.*[11] pointed out that the single-crystal neutron intensity of a type I antiferromagnet with a single-**k** structure (AFI-1**k**) and having an equal domain distribution is the same as for the corresponding multi-**k** structure. In principle, the domain distribution of the single-**k** structure may be changed by applying a uniaxial stress or by cooling the crystal through T_N in a fairly large magnetic field. In high-quality neutron intensity measurements on single crystals of several monopnictides U*X* (*X*=N,P,As,Sb) with stress applied along the [001] direction, it was convincingly shown that this domain distribution in UN was changed in such a manner that the spin structure of this compound can be assigned as a single-**k** case.[11] Moreover, results of muon spin rotation/relaxation/resonance (μSR) measurements[18] also indicated a single-**k** structure for UN. On the other hand, for USb, no change in the domain population was observed under stress (up to 1200 bar) and thus a triple-**k** ordering has been established.[11] Relatively strong domain effects upon an application of magnetic field were observed for UP and UAs in $\chi(T)$ measurements.[19] Applied fields as large as 10 T are required to obtain single domain UP crystals. A subsequent neutron diffraction experiment[20] on UP single crystals cooled through T_N in a field of 2.5 T revealed domain redistribution effects. To our knowledge, no such effects have as yet been observed upon applying magnetic fields in UN crystals. Magnetization measurements[21] performed at 1.3, 20, and 77 K on UN, UP, UAs, and USb in fields up to 40 T showed almost straight-line magnetization curves for UN and USb, while for UP and UAs, a number of magnetic transitions with extremely large hysteresis were observed.

A further fundamental question that has been extensively debated is whether a localized or itinerant description should be used to describe the magnetism of UN. The U-U distance of 3.46 Å in UN is close to the critical value of 3.4 Å given by Hill[22] for the onset of magnetism in actinide systems, whereas this distance is larger for all other U*X* monopnictides as well as for the U*Y* monochalcogenides (*Y*=S,Se,Te). In all of these U*X* or U*Y* compounds, the ordered magnetic moment μ_{or} is smaller than the effective moment μ_{eff}. With the exception of UN, this difference may be approximately accounted for within Hund's rule coupling and crystal-field effects.[23] Amongst these U*X* monocompounds, the difference for UN is exceptionally large, $\mu_{or}=0.75\mu_B$,[10] while $\mu_{eff}=2.66\mu_B$.[2] Therefore, the ratio of the ordered and paramagnetic moments $\xi=\mu_{or}/\mu_{eff}$ of UN (=0.28) lies far away from well-defined limits of Hund's rules (see discussion in Ref. 33). For the f^3 free ion configuration in Russel-Saunders coupling, $\xi=0.90$. This raises the question whether a localized ionic description[1] that works well for compounds such as USb and UTe with their considerably larger lattice parameters is appropriate for UN. Results of inelastic neutron scattering[13,14] and older data of photoemission experiments[15–17] pointed to aspects of nonlocalized behavior associated with the 5*f* electrons in UN.

Inelastic neutron scattering studies[13] indicate that the magnetic response at low temperatures is spread over a considerable frequency range centered on (110) with a large anisotropy gap of ≈3.5 THz (170 K). Although UN is cubic, large anisotropies were also found in its critical scattering.[14] The observed magnetic response in UN has longitudinal polarization without any sharp transverse spin-wave modes. It has been suggested[13] that the observed longitudinal scattering in UN corresponds to excitations across the antiferromagnetic gap, $g(T)$, that appears for $T \leqslant T_N$ at the Fermi level, E_F, in the theory[24] of band magnetism of an antiferromagnet. It is predicted for itinerant magnets that T_N and μ_{or} should have the same pressure dependence since both are directly related to $g(T)$. It has indeed been experimentally observed[12] that T_N and μ_{or} show the same large reduction with applied pressure ($d \log \mu_s/\mathrm{dp} = d \log T_N/dp = -10\ \mathrm{Mbar}^{-1}$). This strongly suggests an itinerant antiferromagnetism in UN. Finally, both an earlier angle-resolved photoemission (ARPES) experiment by Reihl *et al.*[16] and a more recent high-resolution ARPES study by Ito *et al.*[17] on UN and USb crystals reveal for both compounds the dual (itinerant and localized) nature of $5f$ electron bands near E_F with, as expected, a stronger itinerant character in UN than in USb. Nevertheless, according to these authors, some localized character remains in UN and it is reflected, for instance, in the high value of μ_{eff}. One can infer a similar behavior for UN also from recent ultraviolet photoelectron spectroscopy (UPS) studies of thin films prepared under extremely high vacuum.[25] The $5f$ electrons preserve band character, but it is revealed as well that many of the $5f$ states are shifted from E_F toward higher binding energy (BE) of 3–6 eV. This experimental finding is in quite good agreement with preliminary band structure calculations performed previously using different non-full-potential methods.[26–37] On the other hand, some localization is predicted on the basis of the $4f$ core spectra, although these older valence and $4f$ core x-ray photoelectron spectroscopy (XPS) spectra[15] lacked the resolution that is obtained by current experiments.

The present paper reports on the results of modern full relativistic PM band structure calculations, performed by the FPLO (full-potential local-orbital) code,[38] and their comparison with the measured XPS spectra on a single crystal of UN in its PM state. Results are also presented for magnetic and transport measurements pertaining to the main crystallographic axes [100], [110], and [111] of UN single crystals. Previously, $\chi(T)$ was probed[2] by the field applied along the [100] and [110] directions. In this investigation, $\chi(T)$ is studied and compared for the [100], [110], and [111] axes. Former results of $\rho(T)$ were reported only for the [100] direction, but now results for all three main crystal directions are provided. To our knowledge, magnetoresistance (MR) measurements have not been reported so far for either polycrystalline or single-crystalline UN. Results of MR are reported in our paper for the three main directions. Furthermore, the previous studies of thermoelectric power and thermal conductivity, made on sintered powder samples,[39–42] are extended in this paper to single-crystalline samples with the temperature gradient alternatively set along the three main directions.

II. EXPERIMENT

Measurements were performed on single crystals, selected from a batch of material obtained from Battelle Memorial Institute, Columbus, Ohio. Ingots were prepared by nitriding a consumable electrode of depleted uranium under high pressure and these had a resultant structure of UN and U_2N_3. The ingots were subsequently heat treated for 8 h at 1500 °C in a 10^{-5} Torr vacuum to decompose the U_2N_3. Analyses of the crystals indicated near stoichiometry (typical U/N atomic ratio of 1.01), an oxygen content of 290 ppm wt, and a carbon content of 30 ppm wt. The crystals were oriented by x rays using the back-reflection Laue technique and samples for the various measurements were cut using a saw made up of a thin tungsten wire covered with fine BN particles suspended in glycerin.

The XPS spectrum was recorded at room temperature (RT) in a PHI 5700/660 Physical Electronics photoelectron spectrometer using a monochromatized Al $K\alpha$ x-ray source ($h\nu = 1486.6$ eV).[43] The angle between the x-ray beam and the sample surface was 45°. All measurements were performed under ultrahigh vacuum (UHV) condition in the range 10^{-10} Torr on the UN (100) surface, obtained by cleaving the (100) planes *in situ* and immediately after performing the measurements. The energy spectra of the electrons were analyzed by a hemispherical mirror analyzer with an energy resolution of 0.3 eV. E_F was referred to the gold $4f$ at 84 eV BE. The single-crystalline sample of this reactive material, after breaking in UHV condition, produced a spectrum with negligible oxygen and carbon contamination. In the whole region of the measured spectrum (1400–1 eV), there are only small traces of the O($1s$) and C($1s$) peaks at BE of −532 and −290 eV, respectively, and the distinct lack of the peak O($2s$) at −6 eV. The investigated sample did not show signs of surface degradation during the experiment.

Magnetic susceptibility measurements were obtained in the temperature range 1.8–300 K using a Quantum Design MPMS-5 superconducting quantum interference device magnetometer. Resistivity and magnetoresistivity measurements were performed employing a four-probe dc method on samples with typical length $l \cong 4$ mm and cross-sectional area $A \cong 0.7\ \mathrm{mm}^2$. An American Magnetic superconducting coil provided a 8 T field for the MR measurements. Thermoelectric power measurements[44] were made in the steady-state mode on single-crystal platelets that were typically 1 mm thick. A temperature gradient ($1 < \Delta T < 4$ K) was maintained between the two faces of the platelets. For thermal conductivity, bar-shaped samples with $l \cong 4$ mm and $A \cong 1.5\ \mathrm{mm}^2$ were used and a temperature gradient ($3 < \Delta T < 4$ K) was established between the end points of the bar.[45] The thermoelectric power and thermal conductivity were measured over the temperature range 5–300 K. For the latter, the axial stationary heat flow method was applied.

III. THEORY

In the present study of UN, the band structure calculations for the PM state have been performed by the full relativistic version of the FPLO minimum-basis code.[38] In this computa-

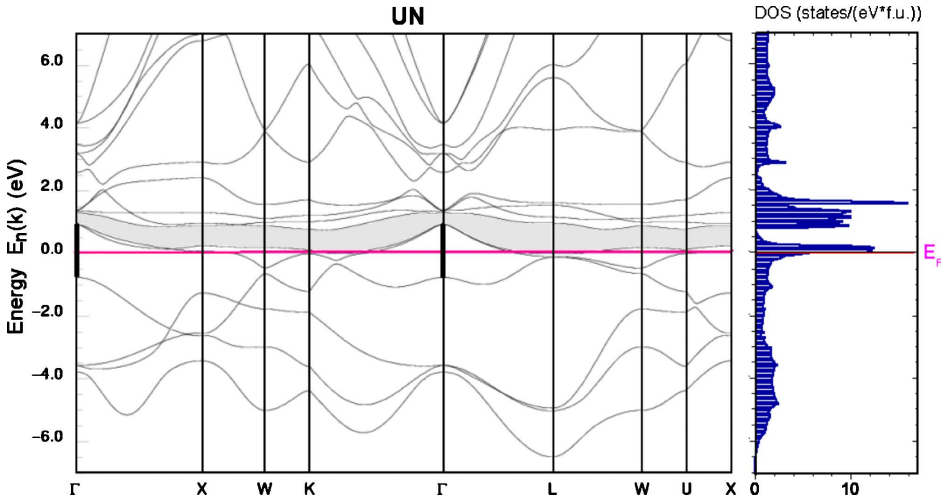

FIG. 1. (Color online) Calculated energy bands $E_n(\mathbf{k})$ and total DOS of UN.

tional method, the four-component Kohn-Sham-Dirac equation, containing implicitly spin-orbit coupling up to all orders, is solved self-consistently. The Perdew-Wang parametrization[46] of the exchange-correlation potential in the local spin-density approximation was applied. UN crystallizes in the common rocksalt structure ($Fm3m$) and for the calculations an experimental value of the lattice parameter $a=4.890$ Å (Ref. 9) was assumed. The following basis sets were used: for U the $5d5f;6s6p6d;7s7p$ and for N the $2s2p;3d$ states were treated as valence states. The high-lying $5d,6s$ and $6p$ semicore uranium states that might hybridize with the $6d$ and $5f$ valence states were included in the basis. The maximum size of the k-point mesh in the Brillouin zone (BZ) was $50\times50\times50$ (2604 k points in the irreducible part of the BZ).

The theoretical band energies $E_n(\mathbf{k})$ as well as the total and partial densities of states (DOSs) were computed, the latter for each atomic site as well as for all the atomic states in the unit cell. In order to compare these calculations with the experimental XPS, the theoretical valence band XPS spectrum was calculated by the standard procedure. Namely, the partial DOSs for the constituent atoms were multiplied by the respective weight factors proportional to atomic subshell photoionization cross sections.[47] The outputs were summed and convoluted with a Gaussian of a full width at half maximum equal to 0.3 eV, simulating the instrumental energy resolution of the analyzer used in the experiment.

IV. RESULTS

A. Electronic structure calculations and x-ray photoelectron spectroscopy

The calculated band energies $E_n(\mathbf{k})$ are displayed in Fig. 1. The bands crossing E_F are dominated by the U $5f_{5/2}$ states, being strongly hybridized with the U $6d_{3/2}$ states, and have a metallic behavior along the ΓK, ΓL, and XW directions. However, there is a pronounced energy gap around E_F along the ΓX line (the gap at the Γ point is marked by a bold bar in Fig. 1), while for the other main symmetry directions, the bands are lying very close to or only slightly cutting E_F. Thus, even small changes in external conditions may influence electronic properties along a given direction.

The calculated total and partial DOSs are shown in Fig. 2. These predict a very broad and complexed contribution from the U $5f$ states clearly visible in the inset of Fig. 2 for the whole energy range, i.e., from 6 eV below E_F and up to 6 eV above E_F. In addition, a minor contribution from these states occurs between 12 and 14 eV below E_F. Due to the spin-orbit splitting (SOS), there are two main U $5f$ peaks, i.e., $5f_{5/2}$ and $5f_{7/2}$, shifted from each other by about 1 eV. Owing to this, a pseudogap at about 0.7 eV above E_F occurs between them. It is interesting to mention that a similar (as to the shape) pseudogap above E_F (see the gray area in Fig. 1) was found for all three uranium monochalcogenides: US, USe, UTe.[48] The lower energy peak of the U $5f_{5/2}$ states cuts the Fermi level, yielding a relatively high DOS at E_F, though the calculated value of the electronic specific heat coefficient $\gamma_b=3.7$ mJ K^{-2} mol^{-1} is much smaller than an enhanced, by a factor of 13, experimental value $\gamma_b=49$ mJ K^{-2} mol^{-1}.[49] No change in the heat capacity has been observed by applying magnetic fields up to 3 T.[49] There are also two broad contributions belonging to the U $5f$ electrons, one between 2

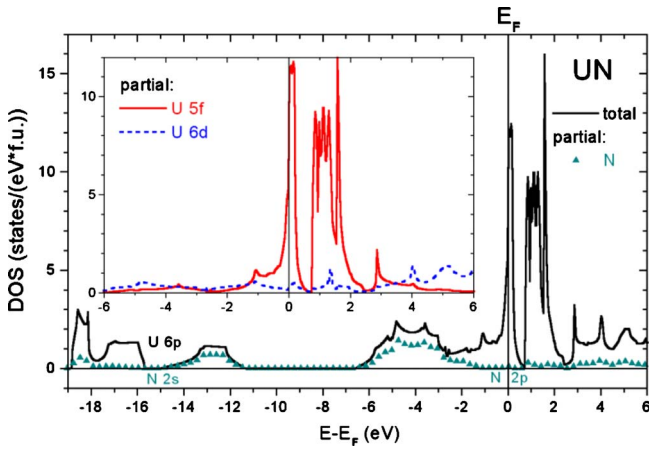

FIG. 2. (Color online) Calculated total and partial DOSs of UN.

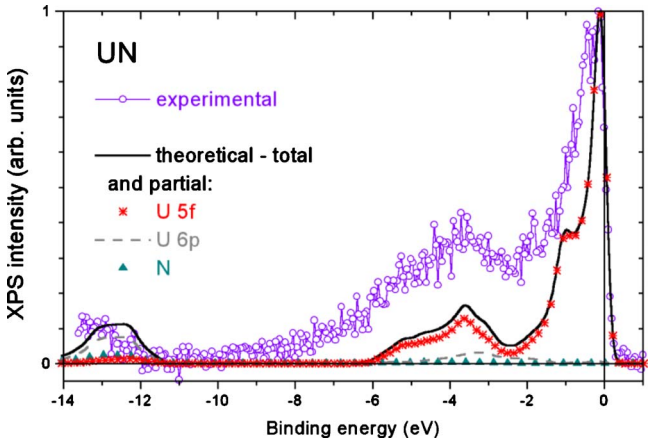

FIG. 3. (Color online) The calculated total valence band XPS spectrum of UN and its partial contributions, compared with the total experimental spectrum after subtracting the background.

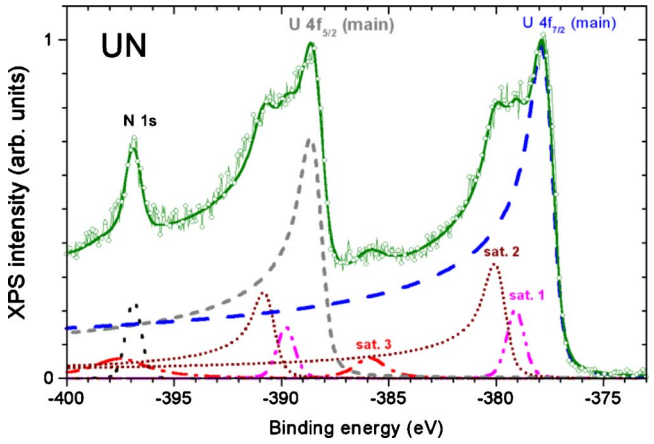

FIG. 4. (Color online) The experimental XPS in the range of the U 4*f* core lines, decomposed into the main sublines $4f_{5/2}$ and $4f_{7/2}$ and their satellites (denoted as sats. 1–3 for the $4f_{7/2}$ line) as well as the N 1*s* line.

and 6 eV below E_F and the other one between 2.5 and 6 eV above E_F. In the same energy range, where the U 5*f* states occur, there is also a pronounced contribution from the U 6*d* states that hybridize with the former. Furthermore, a contribution from the U 6*p* semicore states forms an unusual complex structure. Two deepest energy peaks (among contributions from the theoretical valence-basis electrons), i.e., a narrow one of the highest intensity in full DOS for 25.2–26 eV (not shown) and a broad one for 15.8–18.9 eV below E_F, are created due to SOS of 8 eV from a single broad peak (calculated without SOS). Another broad contribution of less intensity occurs in the range of 11.5–14.3 eV below E_F. Since there is no (in the scale of the figure) contribution from the N states just around E_F, the N 2*p* bands, lying 1.5–6.5 eV below E_F, certainly create the covalent bonding with the U 5*f* and U 6*pd* electrons. Moreover, in the lower energy range of 11–19 eV below E_F, the N 2*s* bands hybridize with the dominant U 6*p* states, which results in the broad valence bands. The electron population analysis shows that the occupation number of the U 5*f* states is reduced from 3 to 2.77 and for the U 6*d* states is increased from 1 to 2.13 electrons per atom, while for the U 7*s* states it is much reduced from 2 to 0.29 electrons with respect to the free atom occupations. In the case of the N atom, the number of the 2*s* states is reduced from 2 to 1.71, and for the 2*p* states, it is increased from 3 to 3.87 electrons. There is a charge transfer of 0.62 valence electron from the U to N atom per f.u.

The calculated valence band XPS spectrum is displayed together with the measured one in Fig. 3. At first, the experimental background was subtracted by the Tougaard method.[50] The large contribution from the U 5*f* states seems to completely dominate not only near E_F but also in the range of 2–6 eV BE below E_F because the contributions from both the U 6*d* and N 2*p* states are determined by extremely low values of the photoemission weight factor and therefore they are invisible in the graph. Contrary to it, a small contribution from the U 6*p* electrons (invisible in the scale of Fig. 2) is relatively enhanced (owing to the weight factors) and thus it is clearly visible in the graph between 1.5 and 5 eV BE below E_F and additionally in the range of 12–14 eV BE (see the dashed line in Fig. 3). In general, all this is in good agreement with the experimental XPS spectrum, especially as to the shape and positions of particular bands. The lack of the O(2*s*) line at about 6 eV of BE below E_F indicates that the sample has been practically not contaminated by oxygen. In conclusion, these data show a highly delocalized character of the U 5*f* electrons and their wide contribution even at energies well below E_F.

The structure of the U 4*f* core lines is presented in Fig. 4. It yields essential information on the final states in the photoemission processes, which turns out to be very complex although well resolved. The U 4*f* line has been decomposed, according to the Doniach-Šunjić theory[51] (after subtracting the background by the Tougaard method[50]), into two highly asymmetric $4f_{5/2}$ (−388.7 eV) and $4f_{7/2}$ (−377.9 eV) main sublines, split by the spin-orbit interaction by 10.8 eV. It appears that each subline is accompanied by as many as three satellites. Unfortunately, the U $4f_{5/2}$ line is distinctly affected by the N(1*s*) contribution, so that only the U $4f_{7/2}$ line can be interpreted unambiguously. A high asymmetry of the main U 4*f* sublines is usually ascribed to U 5*f*-6*d* hybridization effects. In turn, the presence of the symmetric satellite, numbered in the graph as sat. 3 (−385.9 eV), usually occurs in many uranium compounds and hence it was called a 7 eV satellite. Here, it has a small intensity which therefore indicates some decrease of the *f*-*d* hybridization, connected with a slight increase of localization of the U 5*f* electrons (final state $5f^2$). A very high intensity of asymmetric sat. 2 (−380.1 eV), called a 3 eV satellite, has also been observed and this, in turn, may be evidenced as an additional final state [$5f^3$ at the position like that in UO_2 (Ref. 52)]. However, a slight symmetric enhancement of this satellite by contamination of uranium oxides cannot be excluded, although as indicated before, the oxygen content of the sample is low. This is also confirmed by observation of only a very small peak of the O(1*s*) at −532 eV, which is hardly seen in the overall XPS spectrum (not shown) and the lack of a visible anomaly in the valence band XPS around BE of 6 eV below

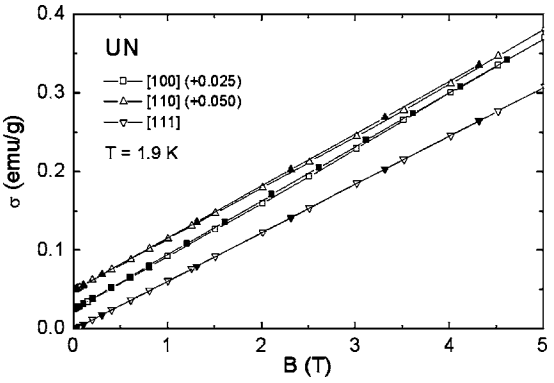

FIG. 5. Magnetization σ at 1.9 K measured along the [100], [110], and [111] axes in applied fields up to 5 T for increasing and decreasing field scans (open and closed symbols, respectively).

E_F. A feature that is completely unique in this study is the observation of a symmetric sat. 1 (−379.1 eV) that is called the 1 eV satellite. Thus, this satellite can be connected with some mixed $5f^3/5f^4$ final states, as discussed in Sec. V.

B. Magnetic susceptibility

Magnetization curves $\sigma(B)$ taken for the [100], [110], and [111] directions of UN at a temperature of 1.9 K are shown up to 5 T in Fig. 5 (note an axis offset), where open symbols indicate measurements taken during the increasing field scan and closed symbols refer to the decreasing field scan.

It is observed that the [111] magnetization curve is linear up to 5 T and it exhibits no hysteresis between increasing and decreasing field scans. For the [100] direction, the initial linear increase of σ with field is only sustained up to 2.5 T, after which it increases with a slightly larger slope. On the other hand, the magnetization curve for this direction, subsequently observed during the decreasing field scan from 5 T, is linear. A subsequent field increase and decrease cycle leaves one on the latter magnetization curve. A similar but somewhat smaller phenomenon is also observed for the [110] direction. A previous study on UN powder performed up to 40 T also indicated an upward deviation from linearity in $\sigma(B)$.[21]

The preceding behavior may be ascribed to the effect of domain wall movements when a magnetic field is applied along either the [100] or [110] direction. Movement of domain walls by a moderate magnetic field is a well-studied phenomenon in AFM Ni0,[53] but to our knowledge, no such effects have been reported for UN single crystals. One expects three types of domains in UN, namely, with spins parallel to the [100], [010], or [001] axis. A reasonable assumption would be to expect equal or nearly equal volumes of these three types of domains in our single-crystal sample. Such an assumption is in line with previous results of neutron scattering[10] and thermal expansion measurements[2] of other UN single-crystal samples.

Application of a field along the [100] direction will, since $\chi_\perp > \chi_\parallel$ for antiferromagnets in general, increase the volume of the [010] and [001] domains at the expense of the [100] domain provided that some wall movement takes place. Similarly, $\mathbf{B} \| [110]$ should tend to increase the volume of the [001] domain. The behavior of the [100] and [110] magnetization curves in Fig. 5 indicates that some small domain wall movement occurs when the field is applied along these directions. The [111] direction, on the other hand, is symmetrically disposed with respect to the cubic axes and hence application of the field along this direction will not favor the increase in size of any of the domains. This is corroborated by the hysteresis free behavior of the [111] magnetization curve.

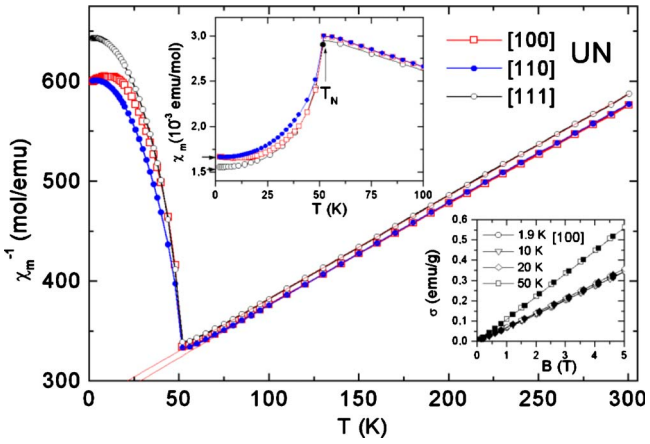

FIG. 6. (Color online) Temperature dependence of the inverse molar susceptibility, $\chi_m^{-1}(T)$, measured in three main directions. Upper inset: Magnetic susceptibility $\chi_m(T)$. Lower inset: Magnetization σ vs an applied magnetic field for increasing and decreasing field scans (open and closed symbols, respectively).

Susceptibility values $\chi_m(T)$ (upper inset), as well as $\chi_m^{-1}(T)$, measured at 0.5 T, are shown in Fig. 6 for three different field orientations along either the [100], [110], or [111] direction. The observed susceptibilities at low temperatures shown in the upper inset of Fig. 6 follow the sequence $\chi_{[110]} \approx \chi_{[100]} > \chi_{[111]}$. The simplest molecular field model[54] for a uniaxial AF predicts that $\chi_\perp = \chi_{T_N}$ at all temperatures in the ordered region and that $\chi_\parallel = 0$ at 0 K. Hence, for an equal domain distribution, this model predicts near 0 K that

$$\chi_{[100]} = \frac{2}{3}\chi_{T_N} = 0.6667\chi_{T_N},$$

$$\chi_{[110]} = \frac{1}{3}(1+\sqrt{2})\chi_{T_N} = 0.8047\chi_{T_N},$$

$$\chi_{[111]} = \sqrt{2/3}\chi_{T_N} = 0.8165\chi_{T_N}.$$

The observed susceptibilities in Fig. 6 do not follow the molecular field expectation. This may simply reflect a breakdown of the molecular field prediction that $\chi_\perp$ is temperature independent.[54] Of more importance is that the observed anisotropy in χ is much less than expected from this simple theory. This result suggests that an ionic localized model may not offer the best description for UN, but that an itinerant approach[12] may be more applicable.

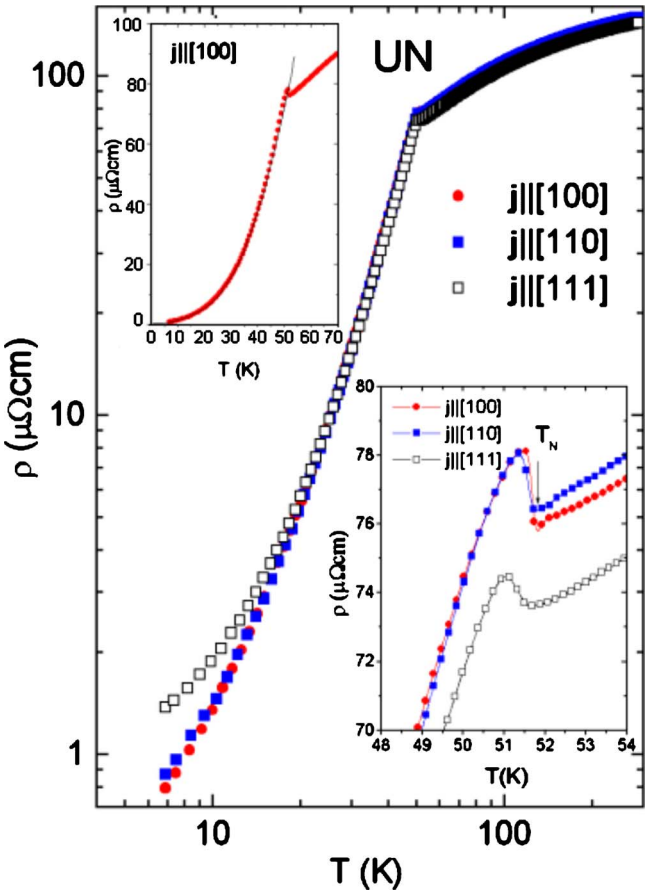

FIG. 7. (Color online) Electrical resistivity $\rho(T)$ of UN vs T measured for $\mathbf{j}$ parallel to three main crystallographic directions indicated in the figure. Upper inset: ρ vs T and the gap fitting (see the text) taken along $\mathbf{j}\|[100]$. Lower inset: The $\rho(T)$ peaks occurring just below T_N.

The data in Fig. 6 follow a modified Curie-Weiss (MCW) relation where the necessity to include a temperature-independent χ_0 term has been well established in previous powder[55] and single-crystal[2] measurements extending in the case of [100] up to 1000 K. A MCW fit to the data in Fig. 6 yields $\chi_0=0.03\times10^{-3}$ emu/mol, $\Theta_p=-294$ K, and $\mu_{\text{eff}}=2.65\ \mu_B$. The values of χ_0, Θ_p, and μ_{eff} given here are averages of the results of least-squares fit calculations of the data for the [100] and [110] directions since it is noted that the [111] paramagnetic results for $\chi_m(T)$ are slightly smaller than those for the [100] and [110] directions. The Θ_p and μ_{eff} values are in excellent agreement with earlier work.[2]

C. Electrical resistivity and magnetoresistivity

Results of electrical resistivity measurements with current flow along the [100], [110], and [111] directions are depicted in Fig. 7. The results for the [100] direction are very similar to our earlier measurements[3] on a different crystal from the same Battelle Memorial batch of crystals. It is also seen that the $\rho(T)$ dependences for the [100] and [110] directions are almost identical. The same holds for the [111] direction, but only down to 20 K. Below this temperature, the resistivity is larger compared with those along the [100] and [110] directions. At 300 K, the ρ values are 148, 150, and 143 $\mu\Omega$ cm, respectively. As previously observed[3,4] for the [100] direction, a small peak in the resistivity below T_N is also visible for the other two directions (lower inset of Fig. 7).

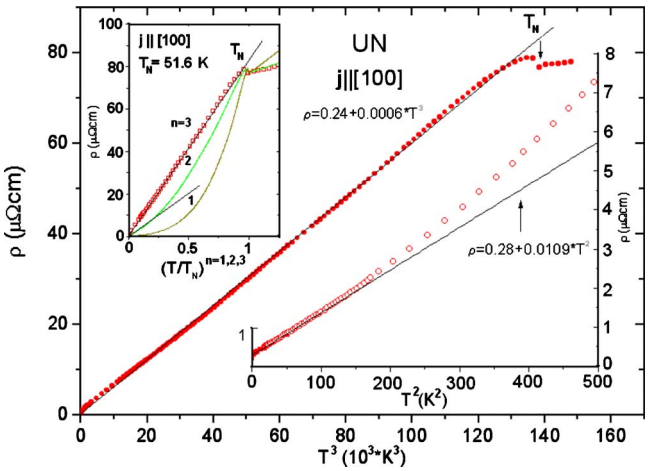

FIG. 8. (Color online) Electrical resistivity ρ vs T^3 along $\mathbf{j}\|[100]$ (closed circles) compared with experimental data. Upper inset: ρ vs T^n $(n=1,2,3)$. Lower inset: ρ vs T^2 (open circles) and a deviation from this behavior at higher temperatures (solid line).

In the case of the [111] direction, the peak height is only 40% of that of the [100] peak. Contrary to it, that of [110] peak is only marginally smaller compared with the [100] peak. It was shown previously[3] that except for a small temperature region near T_N, the $\rho(T)$ dependence in the ordered region scales well with a $1-m_n^2(T)$ dependence, where m_n is the reduced sublattice magnetization of UN, as obtained from neutron scattering.[10] This dependence holds equally well for the present results except for a small deviation from a common behavior along [111] (see Fig. 7). We have also verified that a $\rho(T)\sim T^3$ dependence, as observed by Nasu *et al.*,[4] fits our experimental data for the ordered region (with exception again of the small region below T_N) equally well, as shown in Fig. 8 for $\mathbf{j}\|[100]$.

The physical basis of this empirical observation is not clear at present. In the upper inset of Fig. 8, a comparison with other powers of $\rho(T)\sim(T/T_N)^{n=1,2}$ is also shown.

We initially also tried a spin-wave expression for $\rho(T)$ for a material having a gap in the magnon spectrum:

$$\rho(T)=\rho_0+aT+c_mT^2\exp(-\Delta/T). \quad (1)$$

It gives a good description of the experimental results, but in a very narrow temperature range between 20 and 40 K only. As usual, ρ_0 indicates the scattering of conduction electrons from defects. The experimental ρ_0 value for the studied single crystal of 0.2 $\mu\Omega$ cm is appreciably smaller than that found for a previously studied UN sample [1.8 $\mu\Omega$ cm at 4 K (Ref. 3)]. This gives a residual resistivity ratio for our single crystal of 800. The second term of Eq. (1) describes electron-phonon scattering and the last term describes the scattering of electrons on magnons following a quadratic dispersion and exhibiting an energy gap Δ. The effect of a

crystalline-electric-field splitting, which is characteristic of uranium compounds, introduces a gap in the magnon dispersion relation. The lower inset of Fig. 8 gives the dependence $\rho(T) \sim AT^2$. The straight line with $A=0.011\ \mu\Omega\ \mathrm{cm/K^2}$ is only followed from 0.3 to 12.5 K. Above this temperature, a higher power dependence ($n>2$) is observed. Our value for A is in agreement with similar values of A given in Refs. 56 and 57. The pressure dependence of the A coefficient has recently been determined for UN[57]. It exhibits a maximum value of $0.065\ \mu\Omega\ \mathrm{cm/K^2}$ at 2 GPa.

On the other hand, the resistivity of UN can be explained almost in the whole ordered state according to the theory given by Anderson and Smith:[58]

$$\rho(T) = \rho_0 + AT^2 + BT(1 + 2T/\Delta)\exp(-\Delta/T). \quad (2)$$

Here, the T^2 term is appropriate for Fermi liquid behavior and the last term describes an antiferromagnet with an energy gap Δ. B is related to the exchange coupling. Fitting $\rho(T)$ between 4 K and almost up to T_N for $\mathbf{j}\|[100]$ yields the following parameters: $\rho_0=0.2\ \mu\Omega$ cm, $A=0.016\ \mu\Omega\ \mathrm{cm/K^2}$, $B=12.1\ \mu\Omega\ \mathrm{cm/K}$, and $\Delta \approx 165$ K. Although this equation has originally been derived for a metallic ferromagnet, it has also been successfully applied for a number of uranium-based antiferromagnets, e.g., URu_2Si_2.[59]

A large nonlinear increase in $\rho(T)$ is observed above T_N in all three main crystal directions. This feature was also found before for the polycrystalline[39,40] sample as well as single-crystalline ones.[3,4] We will discuss later on this unusual for the binary uranium compounds feature (see Fig. 9). Figure 9 presents $\rho(T)$, measured on a different UN single-crystalline sample ($\rho_{RT}=169\ \mu\Omega$ cm, $\rho_0 \approx 1.12\ \mu\Omega$ cm) for $\mathbf{j}\|[111]$ (see open squares in Fig. 9) and the same dependence for ThN (solid line) taken from Ref. 60. The ThN sample in this work was obtained by hot pressing finely divided nitride powders ($a_0=5.163$ Å) to a density of 10.6 g/cm^3 which is 92% of the theoretical density. The resistivity of ThN could be described fairly well by the Bloch-Grüneisen formula using a Debye temperature of 300 K, $\rho_0=3\ \mu\Omega$ cm, and $\rho_{RT}=20\ \mu\Omega$ cm.[60] The circles in Fig. 9 represent the difference between the thermal behavior of $\rho(T)_{UN}$ and $\rho(T)_{ThN}$. The remaining $\rho(T)$ curve above T_N is after subtracting the phonon contribution and has still a strong curvature but reaches almost a saturation at RT.

This anomalous behavior, after subtracting the phonon part based on ThN, as well as the spin-disorder part $\rho_m(T)$ is associated with an extra contribution of the crystal field (CF) in UN. Rather than trying to recognize the exact CF splitting of the $5f$ levels, we use a single spacing ($\delta=170$ K) CF model following the analysis of Pinto *et al.*[61] on Nd_2Ni_2Sn. In this model, the CF contribution is described as

$$\Delta\rho_{CF}(T) = \Delta\rho_{CF}(\infty)/\cosh^2(\delta/2T). \quad (3)$$

Taking into account the constant value of $\rho_m(T_N)=85.6\ \mu\Omega$ cm at T_N (=51.6 K) and $\Delta\rho_{CF}(\infty)=63.3\ \mu\Omega$ cm, one obtains a theoretical curve shown in the inset of Fig. 9 (solid line). We used for δ in Eq. (3) the value 170 K close to that ($\Delta \approx 165$ K) taken from the analysis of $\rho(T)$ according to Eq. (2). As seen from this inset, the agreement between the extracted experimental points and the above calculated $\Delta\rho_{CF}(T)$ is quite satisfactory.

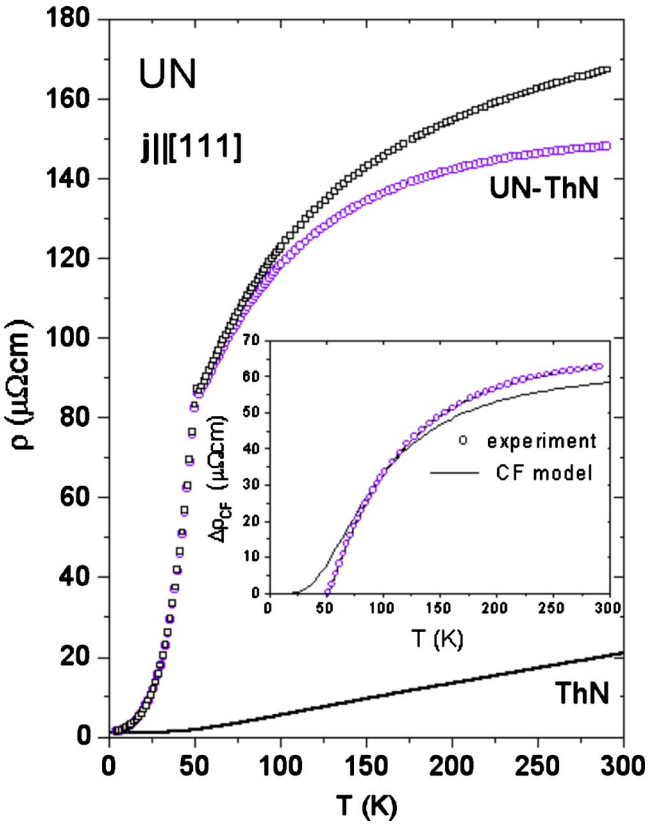

FIG. 9. (Color online) Electrical resistivity, ρ vs T, measured for $\mathbf{j}\|[111]$ for UN (open squares) and for ThN (Ref. 60) (solid line). The differential curve between thermal behaviors of the resistivities of UN and ThN (open circles). The inset shows the experimental CF contribution (open circles) compared with the theoretical CF model predictions (solid line).

It is also valuable to analyze the derivative $d\rho(T)/dT$, especially around T_N for the three main axes. As shown in Fig. 10, this dependence goes through a rounded peak at 47 K in the critical region and is very asymmetric, in agreement with the second-order phase transition in UN. The sharp negative minima determine T_N for all three crystallographic directions. Moreover, at about $T_m=35$ K for all these curves, a small anomaly is observed, however, with unknown origin. It is worthwhile mentioning that a similar anomaly is seen on the $d\rho(T)/dT$ vs T curve presented in Ref. 4. No basic difference has been found between the presented curves in Fig. 10 for the three measured axes.

Results of the temperature dependences of the transverse magnetoresistivity (TMR), defined as $\Delta\rho/\rho_0 = [\rho(B,T)-\rho(0,T)]/\rho(0,T)$, for the [100], [110], and [111] directions, observed in a field of $B=8$ T (applied perpendicular to $\mathbf{j}$), are depicted in Fig. 11. A positive value of TMR as large as 37% is obtained for the [100] and [110] directions at 4.2 K. It is seen that $\Delta\rho/\rho_0(T)$ exhibits distinct differences for the different directions of current in the crystal. In all three cases, $\Delta\rho/\rho_0$ is negative near T_N, as shown in more detail in Fig. 12. The accompanying figures of $\rho(T)$ in Fig.

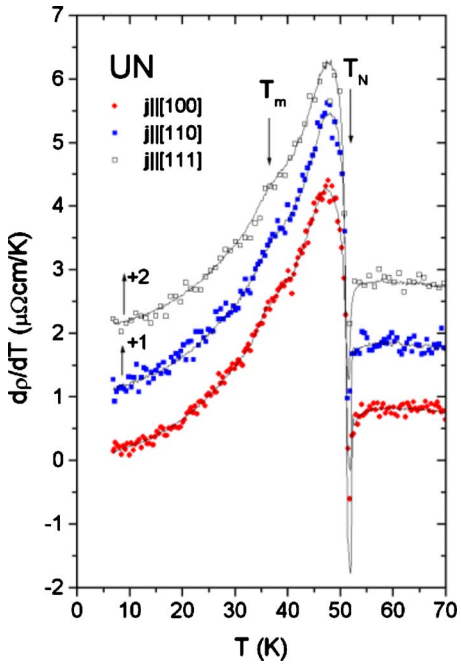

FIG. 10. (Color online) The derivative $d\rho(T)/dT$ vs T calculated for UN with **j** directed along three main axes. Note the offset of the [110] and [111] curves. Note also a sharp negative minimum at T_N for all three cases. T_m marks a small anomaly at 35 K of unknown origin.

12 show how T_N and hence the small peak below T_N shift to a lower temperature when the 8 T field is applied. This leaves some ambiguity in the assignment of T_N from the TMR results.

The rapid change of $\Delta\rho/\rho_0$ for $\mathbf{j}\|[110]$ data to attain positive values below $(T_N-0.6\ \mathrm{K})$ is strikingly different from the initial negative behavior of the $\mathbf{j}\|[100]$ and $\mathbf{j}\|[111]$ data (see Fig. 11). In the latter cases, the TMR becomes positive below 25 and 17 K, respectively.

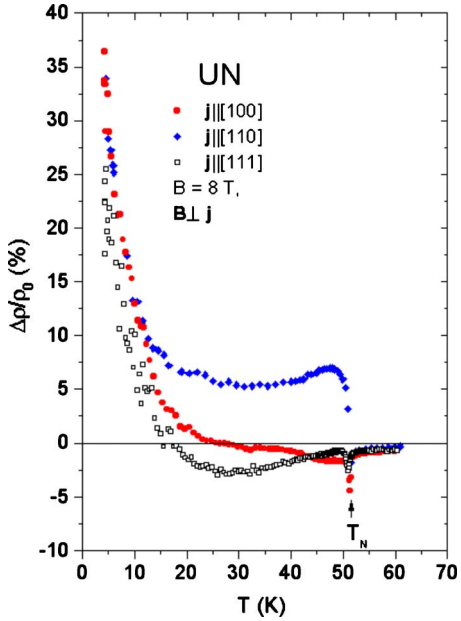

FIG. 11. (Color online) The transverse magnetoresistivity $\Delta\rho/\rho_0$ of UN vs T measured along three main axes.

It is interesting to note that the TMR of UN at 4.2 K is positive and linear in an applied field B up to 8 T (not shown) for the three main crystallographic directions. However, some anisotropy exists due to the different slopes of the $\Delta\rho/\rho_0$ vs **B** dependencies. The largest slope was found for the [110] axis, while the smallest one was found for the [111] axis. On the other hand, the TMR along [100] at higher temperatures is positive and becomes curvilinear following a $B^n(n\leqslant 2)$ dependence at temperatures 10 and 20 K, while for 30 and 40 K, it becomes negative and takes a more complex form (not shown), yielding minima in intermediate strengths of B. Contrary to the above behavior for [100], the TMR along [110] grows almost quadratically with the field in the temperature region from 30 K to T_N. Finally, we found the behavior of the TMR for the [111] direction at higher temperature to be similar to that of the [100] direction. Figure 13 shows the TMR behavior in the vicinity of T_N, i.e., at 51 K. As seen, both TMR curves along [100] and [111] grow negatively with field, while that along [110] grows positively.

D. Thermoelectric power

Results of thermoelectric power (TEP) measurements $S(T)$ with temperature gradient respectively applied along the [100], [110], and [111] directions are given in Fig. 14. The observed values of $S(T)$ for the three directions (in full temperature dependence shown only for [100]) agree very well with one another in the paramagnetic region. The striking feature is here a large value of TEP at RT amounting to slightly more than 50 μV/K. We also show by means of solid lines the $S(T)$ behavior given by Moore *et al.*[39] and Ohmichi *et al.*[40] as measured on a sintered powder UN rod. As seen, the results of Refs. 39 and 40 for the paramagnetic region are in good agreement with our [100] data in a wide temperature range down to 40 K. Below this temperature, our results for all three axes deviate from the former one,[39] as indicated in the inset of Fig. 14. In the antiferromagnetic region, the detailed results for all three directions of the single crystal differ from one another and from that of the polycrystalline sample.[39] Nevertheless, the results share a number of qualitatively similar features. In all instances, a rapid drop is evident when cooling through T_N.

The $S(T)$ values for all directions become negative below 40 K and go through a maximum at about 30 K. In contrary to the polycrystalline data[39] which show a prominent peak at 10 K, only for the [110] and [111] directions does $S(T)$ go through small maxima at 10 K. As required by thermodynamics, one expects $S(T)$ to tend to zero as $T\rightarrow 0$, and this expectation is born out by all our low temperature $S(T)$ curves.

E. Thermal conductivity

Measured values of the thermal conductivity $\kappa_t(T)$ along the [100] and [111] directions are given in Fig. 15 and an appreciable anisotropy is evident at all temperatures. Since

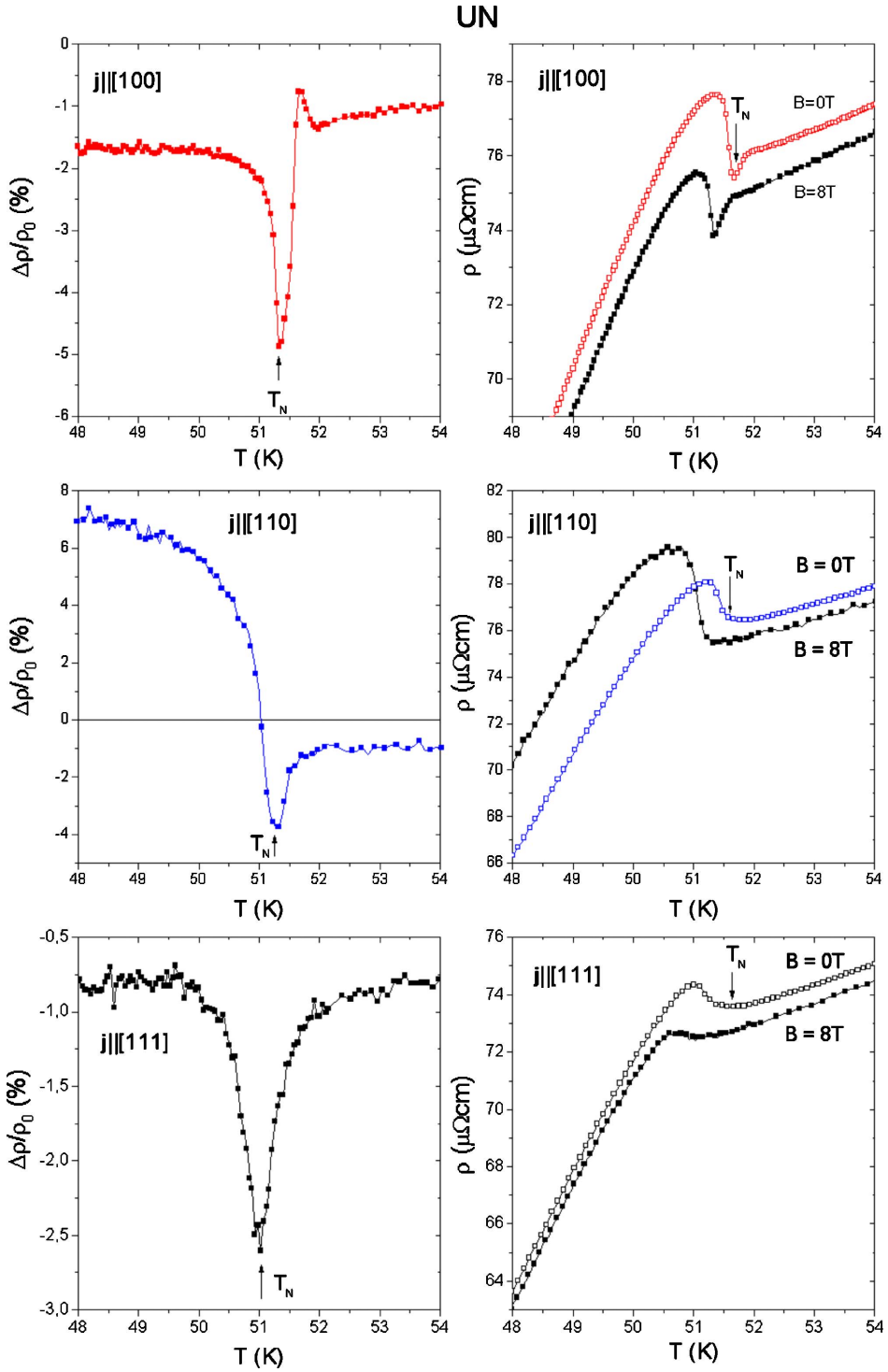

FIG. 12. (Color online) Plots of the resistivity $\rho(T)$ at $B=0$ and 8 T (right hand panels) as well as of the resulting transverse magnetoresistivity $\Delta\rho/\rho_0$ at 8 T (left hand panels) for the [100], [110], and [111] directions in UN for temperatures in the vicinity of the Néel temperature (T_N=51.6 K).

the thermal conductivity in a crystal is described by a second rank tensor, one should not expect it to display anisotropy for a cubic system. It is noted, on the one hand, that these measurements have been performed on different single crystals, although cut from the same batch. Another contributing factor to explain the anisotropy could be the different phonon velocities along the [100] and [111] directions.[62] Also depicted in Fig. 15 as a solid line (Ref. 41) are the low temperature results which are joined to the high temperature data of thermal conductivity (chain line, Ref. 39). Both sets of data were measured on the same sintered powder rod of UN. We have also plotted in this figure a part of the results of Kamimoto *et al.* (Ref. 63). In all these cases, the total thermal conductivity was separated by the authors into electronic κ_e and phonon $\kappa_{\rm ph}$ components. According to Kamimoto *et al.*,[63] $\kappa_{\rm ph}(T)$ goes through a maximum near RT, while κ_e increases almost linearly and crosses the $\kappa_{\rm ph}$ curve at about 450 K. In contrast to the result of Ref. 44 on a polycrystalline sample, our data show structure below T_N. There is a change in slope in $\kappa_t(T)$ at T_N for both directions. Further-

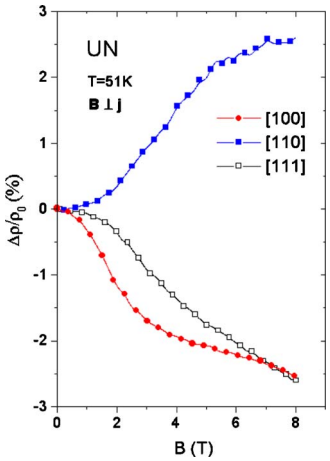

FIG. 13. (Color online) The plot of transverse magnetoresistivity $\Delta\rho/\rho_0$ vs an applied magnetic field B, for UN, taken for the three crystallographic axes at T=51 K, i.e., near the vicinity of T_N (=51.6 K).

more, in both cases, $\kappa_t(T)$ reveals a distinct peak of unknown origin at a lower temperature of about 15 K. On the other hand, the high temperature results of the above authors are in reasonable agreement with our results for the [111] direction in the paramagnetic region.

As a first approximation, the total thermal conductivity was separated into the electronic contribution, κ_e, and phonon contribution, κ_{ph}, using the following equation:

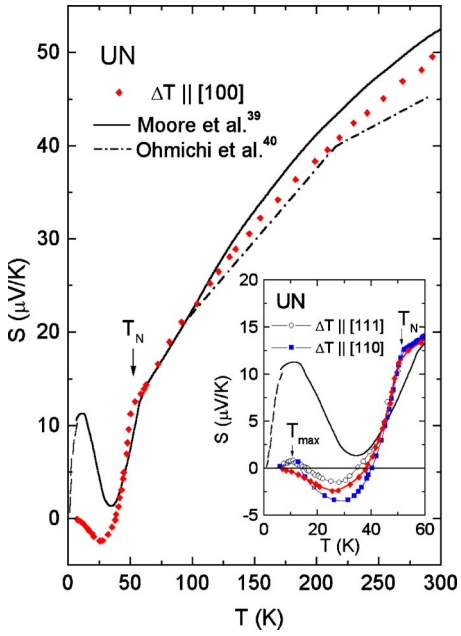

FIG. 14. (Color online) Temperature dependence of the thermoelectric power in UN. No anisotropy in $S(T)$ at higher temperature was detected [only $S(T)$ along [100] is shown]. The solid line and chain lines indicate the results of Refs. 39 and 40, as measured on a sintered powder UN sample. Inset: Thermoelectric power $S(T)$ for the polycrystalline sample (Ref. 39) (solid line) and for the [100], [110], and [111] directions of UN (experimental points).

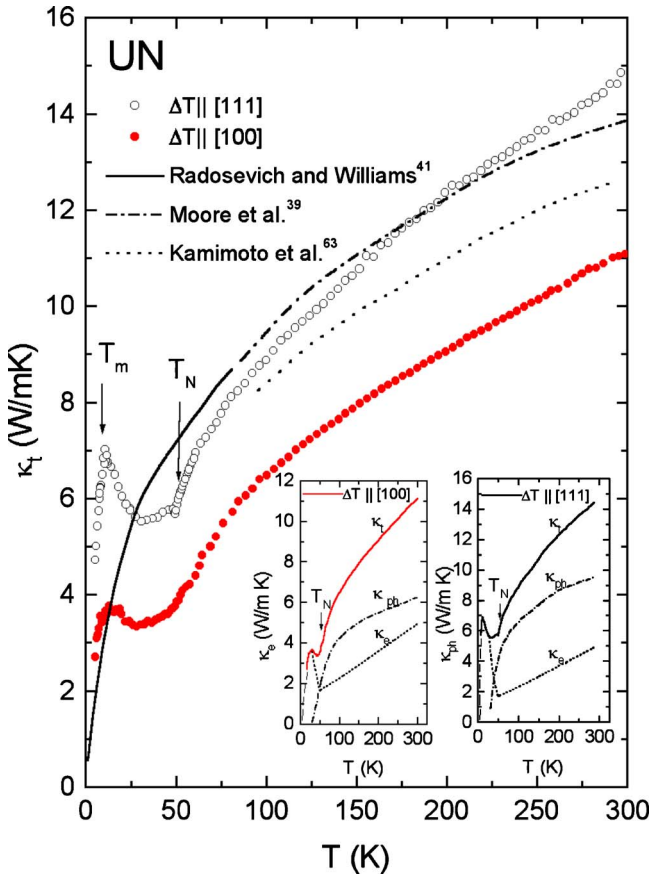

FIG. 15. (Color online) The thermal conductivity along the [100] and [111] directions of UN. Results (Refs. 39, 41, and 63) obtained previously on a sintered powder sample are also shown as lines marked in the figure. The insets display the κ_e and κ_{ph} contribution to κ_t found from Eq. (4) by using our data.

$$\kappa_t = \kappa_e + \kappa_{ph} = L_0 T/\rho(T) + \kappa_{ph}, \tag{4}$$

i.e., by assuming the Wiedemann-Franz law. In Eq. (4), L_0 is the Sommerfeld constant and $\rho(T)$ is the electrical resistivity. The effect of the magnetic characteristics of the material is effectively included in the electronic contribution by using the experimental $\rho(T)$ data in Eq. (4). We show in the insets of Fig. 15 the electronic κ_e and phonon κ_{ph} contributions to $\kappa_t(T)$ derived in this simplified manner for both samples oriented along the [111] and [100] directions.

Finally, Fig. 16 shows the temperature dependence of the reduced Lorentz number L/L_0. At higher temperatures, $L/L_0 > 1$, which indicates that the phonon contribution plays an important role in this temperature range. Contrary to this, the L/L_0 ratio becomes lower than 1 at temperatures below 30–40 K. Note that the electronic contribution to the thermal conductivity, κ_e, estimated from $\rho(T)$ assuming the Wiedemann-Franz law, increases rapidly just below T_N in similar way as it does for UPd_2Al_3.[64] There is a clear upward enhancement in κ_e observed below T_N, compared with the extrapolated values from the high temperature $\kappa_e(T)$ to T_N. This is ascribed to a steep decrease of the electrical resistivity below T_N. Therefore, the electron contribution rapidly

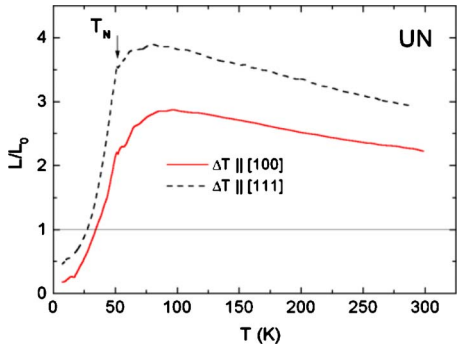

FIG. 16. (Color online) Temperature dependence of the reduced Lorentz number L/L_0 of a UN single crystal, measured in the two directions, [111] and [100], where $L=[\kappa_t(T)\rho(T)]/T(\mathrm{W}\Omega/\mathrm{K}^2)$ is the Lorentz function and $L_0=2.45\times10^{-8}$ $(\mathrm{V}^2/\mathrm{K}^2)$ is the Sommerfeld constant.

rises below T_N to such large values that it unphysically crosses the $\kappa_t(T)$ curve. Also observing similar results, Radosevich and Williams[41] graphically turned down this $\kappa_e(T)$ rise to disallow such a crossing. On the other hand, at high temperature above T_N, κ_e is smaller than κ_{ph} due to the increase in the electrical resistivity in this temperature region and then the heat current is carried mainly by phonons.

V. DISCUSSION

A. Electronic structure calculations and x-ray phoelectron spectroscopy

One of the most interesting results for UN, obtained in this paper, is an observation of the extremely broad and complex contribution from the U $5f$ states that plays a role in forming both metallic (due to hybridization of U $5f$-$5f$ and U $5f$-$6d$ states) and covalent (hybridization of U $5f$ and N $2p$) bonding. Such a behavior of the U $5f$ states has already been suggested by results of non-full-potential band structure calculations, performed by Brooks,[29,31–34] employing the linear muffin tin orbital (LMTO) method. Also, Weinberger *et al.*,[35] using the relativistic Korringa-Kohn-Rostocker (KKR) scheme, as well as recently Kotomin *et al.*,[37] applying non-full-relativistic pseudopotential codes, have pointed to mixed covalent and metallic character of bonding in UN. Unfortunately, none of these authors has presented DOS for the full relativistic case. The scalar relativistic (without the spin-orbit correction) DOS, shown by Brooks in Refs. 31, 33, and 34, can be considered as only a crude approximation. Nevertheless, they agree with our full-potential relativistic FPLO results (Fig. 2) as to the position of the bottom (going down to about −7 eV) of the highest in energy valence bands. Note that the latter overlap with the conduction bands. Also, the total contribution of the U $5f$ states, presented in Ref. 31 for UN, is quite broad, ranging from about −5 to 2 eV, but we observe it even deeper in energy, i.e., at least down to about ~−6 eV. To our knowledge, such a case of $5f$ DOS has not been reported so far in the literature also for other uranium compounds. According to Cooper *et al.*,[65] the $5f$ wave spectral functions can be considered as consisting of two parts: The localized $5f$ waves in the form of a narrow peak (in an energy scale) corresponding to the atomic core regions (in the real space) and the itinerant $5f$ waves outside the peak for the extended (outside core) regions. However, it is rather difficult to make a sharp division of the $5f$ waves into the localized and itinerant ones.

A relatively high intensity contribution from the $5f$ states is visible for UN at E_F in both scalar and our full relativistic DOS (Fig. 2). In addition, our results show explicitly the SOS of the U $5f$ states with a magnitude of 1 eV, which is typical for uranium compounds, compared to a value of 0.77 eV given by Brooks for UN in Ref. 34. Moreover, the energy range for the contribution from the N $2p$ states, having a gap around E_F, was similar to that obtained in our calculations. Partial DOSs for other states in UN were not presented by either Brooks or other authors. Although Brooks published[32] full relativistic band energies, $E_n(\mathbf{k})$, these are only along the ΓX direction. The band structure along the ΓX line is quite similar to our results, particularly as to an energy gap that is maximum at the Γ point (from −0.8 to 0.85 eV, marked by a bold bar in Fig. 1). The lowest band above E_F strongly falls down along the ΓX line and at the X point it almost coincides with E_F. Also, a behavior of high-lying valence bands is comparable to earlier results. The subsequent band energies obtained in our work are shifted by about 0.3 eV toward lower energies. A much greater shift of the bands along ΓX was reported by Weinberger *et al.*[35] using the relativistic KKR method. The band structure presented by these authors differs, however, from our and Brooks' results mainly around the Γ point. The discrepancies at this point are as to both a behavior of unoccupied bands and a considerably smaller size of the energy gap around E_F. Furthermore, our DOS and $E_n(\mathbf{k})$, taken in the lower energy range 11–19 eV below E_F (not shown), reveal wide valence bands dominated by the U $6p$ electrons that hybridize with the N $2s$ electrons, creating the covalent bonding. This is in quite good agreement with the analysis of the KKR results made by Weinberger *et al.*[35] Finally, the scalar spin-polarized DOSs, recently shown by Kotomin *et al.*,[37] were based on less accurate pseudopotential methods. They nevertheless agree quite well with our results, but only as to the N $2p$ contributions and the presence of the U $5f$ states at E_F.

Recent photoelectron spectroscopy investigations of both valence band and $4f$ core states in UN films[25] have confirmed that the U $5f$ electronic states are predominantly itinerant in character, showing a relatively high DOS at the E_F. Although the $5f$ electrons preserve a band character, it was nevertheless shown that the majority of the $5f$ states are shifted by 3–6 eV from E_F toward higher BE. Moreover, general good agreement was achieved between the measured position of the N $2p$ band and that predicted by the results of LMTO[31] and our FPLO calculations presented in this paper. On the basis of older photoelectron XPS and UPS measurements[15] and the more recently reported temperature-dependent ARPES studies,[16] ranging from 33 to 75 K, mainly an itinerant-$5f$-electron character has been postulated, which is in agreement with our high-resolution experimental XPS spectrum (Fig. 3). The authors of the latter work

observed a strong, dispersive peak, i.e., emerging at about −0.7 eV in addition to the sharp peak at E_F. This peak, arising from the band-gap state, decreased as T was raised above T_N. In the AF phase, the uppermost valence band below E_F can be schematically folded back into the new Brillouin zone, creating some new state at the Γ point and an energy gap at the new zone boundary (at $0.5|\Gamma X|$). In turn, Norton *et al.*[15] improperly ascribed a broad contribution between 2 and 6 eV BE in the XPS valence band, measured for the same energy, i.e., Al Kα (1486.6 eV) as for our XPS, only to the U 6*d* and N 2*p* states. Our FPLO calculations predict that both these contributions should be canceled by the photoemission weight factors and thus be completely invisible. Instead, the U 5*f* states dominate in this energy region and in addition, the U 6*p* electron contribution is also well pronounced. This is confirmed by the good agreement between our calculated and measured total XPS. The latest study of high-resolution ARPES, performed for single-crystalline UN,[17] indicates the dual (itinerant and localized) nature of the 5*f* electron bands near the E_F. Hence, some localized character seems to remain at higher temperatures in UN, in agreement with the previous predictions[15] made on the basis of the 4*f* core spectra, though the latter were of least quality. In contrary, our high-quality 4*f* core XPS measurements presented here (Fig. 4) allow for detailed analysis of the 4*f* line in UN. To our surprise, it appears to have a very complicated structure with as many as three satellites per each of U $4f_{5/2}$ and $4f_{7/2}$ main sublines. The 7 eV satellite (sat. 3 in Fig. 4) has been often observed in other uranium compounds[66] and its small intensity in our case can be ascribed to the weak localization of the U 5*f* electrons ($5f^2$ final state). The most pronounced asymmetric 3 eV satellite (sat. 2) is usually interpreted for samples without oxygen contamination as evidence for an additional final state ($5f^3$).[48,52,65] Nevertheless, this satellite is often ascribed to contamination by UO_2. It is interesting that the 4*f* spectrum in $UNiSb_2$, where the investigated sample is completely without traces of oxygen, displays a pronounced 3 eV peak (Fig. 8 in Ref. 43). In turn, the most interesting feature is a symmetric 1 eV satellite (sat. 1), recently observed for some probably mixed-valent compounds.[66,67] It can be considered as being connected with the $5f^3/5f^4$ final states. Such a complex structure of the deconvoluted U 4*f* core lines most likely indicates the dual character of the U 5*f* states reflected in the 4*f* spectra, with a possibility of a fluctuation between the hybridized $5f^26d^1$ and almost local $5f^3$ states.[68]

B. Magnetic susceptibility

Low temperature magnetization isoterms along [100] and [110] direction of UN show a small hysteresis that has been ascribed to very limited domain wall movements. The overall effect even in the highest field of 5 T would amount an equal distribution of the three types of domains ([100], [010], and [001]) in the crystal. The domain structure and domain wall movements are not considered to be significant factors when interpreting the results of transport properties in the following sections.

The paramagnetic susceptibility follows a modified Curie-Weiss relation which includes a temperature-independent χ_0 term. The observed Weiss constant $\Theta_p=-249$ K and effective moment $\mu_{\text{eff}}=2.65\mu_B$ is in good agreement with a previous investigation.[2]

C. Transport properties

1. Electrical resistivity and magnetoresistivity

In spite of considerable research effort undertaken on UN,[1] no clear understanding of its transport properties has been achieved up to now. In general, this results from the more extended nature of 5*f* electrons and their strong tendency to hybridize with the U 6*d* and nitrogen *p* electrons, giving rise to a complex electrical behavior. The most remarkable feature of the resistivity is the hump below T_N found for all the main directions measured (see lower inset of Fig. 7). Previously, such a small hump has been observed in several systems including Cr, γ-Fe, α-Mn, Dy, and recently in several uranium-based antiferromagnets such as tetragonal URu_2Si_2,[69] hexagonal $UNiGa_5$,[70] and cubic UGa_3.[70] Band structure calculations and de Haas–van Alphen data of $UNiGa_5$ (Ref. 70) revealed the presence of the Fermi surface (FS) nesting which is a condition for the formation of a spin-density-wave (SDW) gap. This results in a decrease of charge carriers and hence an increase in resistivity just below T_N. Thus, the charge carrier concentration though decreasing the temperature below T_N does not vanish and the compound stays metallic below T_N. In the latter two compounds as well as in cubic UN (Ref. 3) and UGa_3,[71] a small hump in $\rho(T)$ just below T_N is reminiscent of the SDW formation. Both the latter cubic compounds are supposed to have an itinerant-5*f*-electron nature at least in the ordered state. However, in some aspects, there is a difference between $UNiGa_5$ and UGa_3, on the one hand, and UN, on the other hand. For the two former compounds, $\chi(T)$ in the paramagnetic range is almost temperature independent, while for UN, $\chi(T)$ follows a normal Curie-Weiss behavior. Hence, taking into account the paramagnetic range only, UN cannot be classified as having delocalized U 5*f* electrons. Following the earlier studies of Robinson and Erdös,[72] it is more likely to assume a transformation into the band behavior of some 5*f* electrons just at T_N. It is also found from high-resolution temperature-dependent photoemission measurements of UPd_2Al_3 (Ref. 73) that the behavior of the U 5*f* electrons indicates the "dual" character. In this case, there is an increase in the degree of delocalization of the 5*f* electrons with cooling and a more localized behavior of these electrons at high temperature.

It is also possible to explain the existence of a hump in $\rho(T)$ below T_N to the interplay of two competing mechanisms, as proposed in the case of UNi_2Ge_2.[74] The basic idea is the reduction of the number of effective conduction electrons due to the spin-wave gapping of the FS at T_N caused by the magnetic ordering, on the one hand, and the reduction of the spin-disordered scattering by lowering the temperature, on the other hand. The former mechanism increases the resistivity, while the latter one decreases it. The gapping of the FS is due to the introduction of the new magnetic Brillouin zone that is only half of the size of that in the paramagnetic state (see Refs. 3 and 16). Hence, the effects of hybridization

of $5f$ electrons in the uranium compounds of the simple rocksalt structure cause that they behave typical of a two-dimensional system, although the material is cubic.

It is worthwhile mentioning that in view of the possible "duality" of the $5f$ electrons, one should also consider the localized aspects of the $5f^2$ electron configuration even if these are weakly hybridized with the U $6d$ or ligand electrons. Nevertheless, they experience the relatively strong crystal field of the octahedrally surrounded ligands. As shown by Lemmer and Lowther,[75] the $5f^2$ configuration satisfactory accounts for the temperature dependence of the sublattice magnetization, m_n, of UN in the ordered region, as well as the paramagnetic susceptibility between T_N and 1000 K, being more in line with the results of Ref. 55 than of other studies. For example, the ordered moment value was accounted for in terms of a simple model of two levels, separated by $\Delta=177$ K. It could not be explained by assuming the U^{3+} ($5f^3$) ion. Such a two level model has been applied in the present paper as well (see the inset of Fig. 9) to explain an excess of the resistivity, $\Delta\rho_{\mathrm{CF}}(T)$, in the paramagnetic state. Satisfactory agreement between theoretical and experimental curves is obtained with a single crystal field spacing $\delta=170$ K. A similar model, but using two levels, Γ_1 and Γ_4 (singlet and triplet, respectively), was considered by De Novion[76] to explain the magnetic heat capacity, $C_m(T)$, and magnetic part of the electrical resistivity, $\rho_m(T)$, in the ordered and paramagnetic regions of UN. This author found an energy splitting of these levels, $E_{1,4}=185$ K and 103 K from the heat capacity and magnetic resistivity, respectively. It follows from the above discussion that the spin-wave gap ($\Delta \approx 165$ K) and the energy difference $\delta=170$ K found in our fit of $\Delta\rho_{\mathrm{CF}}(T)$ as well as the values derived by the authors of Refs. 75 and 76 all have comparable values. These arguments are also supported by the magnetic entropy which was found by separating the lattice contribution from the total heat capacity by using $C_p(T)$ of ThN (see Ref. 1, Fig. II.69). At T_N, $\Delta S_m=0.51\mathrm{R}\ln 2$. This is a too large value for a band description of the $5f$ electrons in UN, but it is of an appropriate magnitude for a singlet ground state. Thus, for such a ground state system, Grunzweig-Genossar[77] derived an equation for calculating the magnetic entropy and determined graphically its dependence on the ratio $X=$the level separation δ divided by T_C or T_N. In our case, $X=3.3$ which leads to $\Delta S_m=0.4\mathrm{R}\ln 2$. The missing entropy may be associated with the itinerancy of $5f$ electrons, as for many itinerant systems the entropy is roughly equal to $(0.1-0.2)\mathrm{R}\ln 2$.

The transverse MR, in which the direction of the magnetic field and the current are perpendicular to each other, can provide some information on the overall topology of the FS. In the case of UN at moderate temperatures, the TMR increases nearly quadratically with the applied magnetic field but depends on the current direction relative to the crystal orientation. This suggests that UN could be a compensated metal. At temperatures between 20 K and T_N, the complex behavior of the TMR occurs. It is conjectured that this may be caused by the existence of also another component leading to the occurrence of broad negative minima in the TMR in magnetic fields of about 4–5 and 6–7 T for the [100] and [111] directions of the current. On the other hand, TMR for $\mathbf{j}\|[110]$ at temperatures $T\geqslant 30$ K is almost at all temperatures positive and changes quadratically with $\mathbf{B}$, yielding higher values at 8 T on proceeding toward T_N. In the paramagnetic range, the TMR changes with $\mathbf{B}$ typically as for Kondo-like materials for all current directions. The overall temperature dependence of the TMR in UN is completely unusual (see Figs. 11 and 12). However, the sharp negative dips at T_N again prove the existence of compensation of holes and electrons ($n_h=n_e$) in this compound. It is interesting to note that the humps in $\rho(T)$ still exist in an applied field of 8 T, although they become somewhat smaller (see Fig. 12).

2. Thermoelectric power

In general, the TEP can be expressed as the sum of three contributions:

$$S_t = S_d + S_{\text{ph-drag}} + S_{\text{mgn-drag}}, \tag{5}$$

where S_d is due to diffusion of electrons and the other two are phonon and magnon drags. We think that the low temperature maximum in $S(T)$ at 10 K may be of a magnon-drag origin that comes from the electron-magnon interaction, which in turn drives $S(T)$ to a maximum for temperatures at about $T_N/10<T<T_N/5$. In the case of electron-phonon interaction, taking into account the Debye temperature of UN, $\Theta_D(=324\ \mathrm{K})$,[49] any phonon-drag peak should arise at least above 32 K. As Fig. 14 indicates, at this temperature, $S(T)$ is negative and displays a minimum for all the principal crystal directions. However, the most important S_d part is usually expressed as follows:

$$S_d = (\Pi^2 k_B^2 T/3e)\,\{\partial \ln N(E)/\partial E + \partial \ln \tau(E)/\partial E\}|_{E=E_F}, \tag{6}$$

where $N(E)$ is the DOS near E_F and τ is the relaxation time of the scattered conduction electrons. It is clear that in the case of a sharp maximum at E_F in the $N(E)$ dependence, one should expect a distinct change in the total $S_t(T)$ function. A lot of magnetically ordered materials do not show such a distinct change in the thermoelectric power, at the ordered temperature, as is observed for UN. Of several studied uranium compounds, only for UPdSn and UCuSn (Ref. 78) does the TEP have some similarity to that of UN. The TEP curves below T_N of these two compounds change their slopes, drop to negative values, and attain minima at 20 and 35 K, respectively. This behavior was attributed by the authors of Ref. 78 to a narrow feature in the DOS near E_F, associated with the $5f$ electrons. According to these authors, the behavior below T_N indicates that a predominant holelike part of the FS is being affected due to the magnetic ordering. The TEP becomes more negative as the electronlike portion of the FS becomes less compensated by the holes. This picture is consistent with our thermal conductivity results, where in the insets of Fig. 15 we have pointed out the low temperature rapid increase in the electron contribution to $\kappa_t(T)$ and the simultaneous vanishing of the phonon part just below T_N. On the other hand, this dramatic reversal in $S(T)$ of UN below T_N, as described above, can also be compared to the SDW transition (e.g., Ref. 79). Furthermore, in an antiferromagnetic Cr alloy doped slightly with Al, a similar strong

anomaly in $S(T)$ was revealed below T_N.[80] The earlier observed elastic anomalies in UN just below T_N,[5] which are similar to elastic anomalies associated with the SDW transition in Cr,[81] might possibly reflect on the presence of a collective SDW mode in UN. Such a possibility of the SDW presence in tetragonal UCu_2Si_2 at temperatures between T_C and T_N has recently been pointed out clearly by Honda *et al.* in their neutron scattering studies.[82]

3. Thermal conductivity

In general, the total measured thermal conductivity of a magnetic specimen is usually expressed as a sum of electronic, κ_e, phonon, κ_{ph}, and magnon, κ_m, components. The $\kappa_e(T)$ contribution is caused by the scattering of conduction electrons on lattice imperfections, phonons, and magnetic moments. The $\kappa_{ph}(T)$ contribution comes from collisions of phonons on impurities and/or defects present in the lattice, conduction electrons, other phonons, and magnetic moments. In turn, the κ_m component, usually being difficult to separate, is due to interactions of spin-wave excitations, with both electrons and phonons. In magnetically ordered region, the phonon contribution is then enlarged by the magnon component. However, its influence is clearly seen as a rapid upturn in the $\kappa_t(T)$ curves of UN at and below T_N and a sharp maximum at $T \approx 15$ K. At low temperatures below T_N, the scattering of electrons becomes dominant. In contrast, at elevated temperatures, the scattering of both electrons and phonons, being of elastic and inelastic character and described by the normal- and Umklapp-type processes, are equally important. Usually, the thermal conductivity $\kappa_t(T)$ in the paramagnetic range is nearly proportional to T and is expected to show a tendency to saturation at high temperatures. In fact, such a behavior of $\kappa_t(T)$ in the paramagnetic region is observed for UN. Nevertheless, in the paramagnetic region, the phonon contribution increases with the increase in temperature, then goes through a maximum above RT,[39] and keeps its dominance over $\kappa_e(T)$ up to 450 K.[64] As shown by Bhattacharjee and Coqblin,[83] the scattering of the conduction electrons on localized magnetic moments usually plays a substantial role in compounds exhibiting a strong crystal-field effect, as it does in $UCuP_2$ and $UCuAs_2$.[84]

VI. CONCLUSIONS

The above discussion is focused mainly on the "dual" and SDW-like behavior of the $5f$ electrons in UN. Itinerant or localized behavior or both is observed, depending on the properties which are examined. A very similar situation to the case of UN was reported on UPd_2Al_3,[85] UGa_3,[71] $UNiGa_5$,[70] and URu_2Si_2.[59] The results of XPS and band structure calculations obtained at RT cannot give a final solution to the above problems. This problem is also addressed by recent measurements of optical and magneto-optical properties of UN,[86] yielding results in general agreement with our electronic structure results. However, UN requires further intensive studies using other modern methods such as synchrotron radiation (SR) and ARPES. Especially, magnetic x-ray scattering studies using SR can be utilized to further investigate the magnetic structure and possibly presence of new magnetic phases such as the SDW in this compound. The various anomalies observed in the $\Delta\rho/\rho_0(T)$, $d\rho(T)/dT$, $S(T)$, and $\kappa(T)$ curves in the ordered state suggest that the magnetic structure of UN may be more complicated than the AFI-1**k** structure in certain temperature regimes below T_N. Without knowledge of the full magnetic structure, an interpretation of the measured properties is somewhat limited.

ACKNOWLEDGMENTS

We thank A. Stępień-Damm for making orientation of UN crystals, T. Durakiewicz for kind remarks after reading the paper, and B. Badurski and R. Gorzelniak for their technical assistance.

[1] R. Troć, *Pnictides and chalcogenides III (Actinide monopnictides)*, edited by H. P. J. Wijn, Landolt-Börnstein, New Series, Group III, Vol. 27 (Springer-Verlag, Berlin, 2006).
[2] C. F. Van Doorn and P. de V. du Plessis, J. Low Temp. Phys. **28**, 391 (1977).
[3] C. F. van Doorn and P. de V. du Plessis, J. Low Temp. Phys. **28**, 401 (1977); P. de V. du Plessis and C. F. van Doorn, Physica B & C **86-88B**, 993 (1977).
[4] S. Nasu, T. Kurasawa, H. Matsui, M. Tamaki, and M. Okuda, in *Plutonium and Other Actinides*, edited by H. Blank and R. Lindner (North-Holland, Amsterdam, 1976), p. 515.
[5] C. F. van Doorn and P. de V. du Plessis, J. Magn. Magn. Mater. **5**, 164 (1977).
[6] M. Yoshizawa, B. Lüthi, T. Goto, T. Suzuki, B. Reuker, A. de Visser, P. Frings, and J. J. J. M. Franse, J. Magn. Magn. Mater. **52**, 413 (1985).
[7] M. D. Salleh, J. E. Macdonald, G. A. Saunders, and P. de V. du Plessis, J. Mater. Sci. **21**, 2577 (1986).
[8] J. A. C. Maples, C. F. Sampson, F. A. Wedgwood, and M. Kuznietz, J. Phys. C **8**, 708 (1975).
[9] H. W. Knott, G. H. Lander, M. H. Mueller, and O. Vogt, Phys. Rev. B **21**, 4159 (1980).
[10] N. A. Curry, Proc. Phys. Soc. London **86**, 1193 (1965).
[11] J. Rossat-Mignod, P. Burlet, S. Quezel, and O. Vogt, Physica B & C **102B**, 237 (1980).
[12] J. M. Fournier, J. Beille, A. Boeuf, C. Vettier, and A. Wedgwood, Physica B & C **102B**, 282 (1980).
[13] W. J. L. Bagers, A. F. Murray, T. M. Holden, E. C. Svenson, P. de V. Du Plessis, G. H. Lander, and O. Vogt, Physica B & C **102B**, 291 (1980); T. M. Holden, W. J. L. Buyers, E. C. Svensson, and G. H. Lander, Phys. Rev. B **30**, 114 (1984).
[14] T. M. Holden, W. J. L. Buyers, E. C. Svensson, and G. H. Lander, Phys. Rev. B **26**, 6227 (1982).
[15] P. R. Norton, R. L. Tapping, D. K. Creber, and W. J. L. Buyers, Phys. Rev. B **21**, 2572 (1980).
[16] B. Reihl, G. Hollinger, and F. J. Himpsel, Phys. Rev. B **28**, 1490

(1983); B. Reihl, J. Less-Common Met. **128**, 331 (1987).
[17] T. Ito, H. Kumigashira, S. Souma, T. Takahashi, and T. Suzuki, J. Magn. Magn. Mater. **226-230**, 68 (2001).
[18] K. H. Münch, A. Kratzer, G. M. Kalvius, L. Asch, F. J. Litterst, and K. Richter, Hyperfine Interact. **78**, 435 (1993).
[19] G. Busch, F. Hullinger, and O. Vogt, J. Phys. (Paris), Colloq. **40**, 62 (1979); O. Vogt, Physica B & C **102B**, 206 (1980); O. Vogt, P. Wachter, and H. Bartholin, *ibid.* **102B**, 226 (1980); G. Busch and O. Vogt, J. Less-Common Met. **62**, 335 (1978).
[20] P. Burlet, S. Quezel, J. Rossat-Mignod, and R. Horyń, Solid State Commun. **55**, 1057 (1985).
[21] C. J. Schinkel and R. Troć, J. Magn. Magn. Mater. **9**, 339 (1978).
[22] H. H. Hill, in *Plutonium and Other Actinides*, edited by W. N. Miner (American Institute for Metallurgical Engineers, New York, 1970), p. 2.
[23] S.-K. Chan, J. Phys. Chem. Solids **32**, 1111 (1971).
[24] P. A. Fedders and P. C. Martin, Phys. Rev. **143**, 245 (1966).
[25] L. Black, F. Miserque, T. Gouder, L. Havela, J. Rebizant, and F. Wastin, J. Alloys Compd. **315**, 36 (2001).
[26] M. Erbudak and J. Keller, Z. Phys. B **32**, 281 (1979); J. Keller and M. Erbudak, J. Phys. (Paris), Colloq. **40**, C4-22 (1979).
[27] M. S. S. Brooks and D. Glötzel, Physica B & C **102B**, 51 (1980).
[28] M. S. S. Brooks and D. Glötzel, J. Magn. Magn. Mater. **15-18**, 873 (1980).
[29] M. S. S. Brooks, J. Magn. Magn. Mater. **29**, 257 (1982).
[30] M. S. S. Brooks and P. J. Kelly, Phys. Rev. Lett. **51**, 1708 (1983).
[31] M. S. S. Brooks, J. Phys. F: Met. Phys. **14**, 639 (1984).
[32] M. S. S. Brooks, J. Phys. F: Met. Phys. **14**, 857 (1984).
[33] M. S. S. Brooks, J. Magn. Magn. Mater. **47-48**, 260 (1985).
[34] M. S. S. Brooks, Physica B & C **130B**, 6 (1985).
[35] P. Weinberger, C. P. Mallet, R. Podloucky, and A. Neckel, J. Phys. C **13**, 173 (1980).
[36] G. H. Schadler and R. Monnier, Z. Phys. B: Condens. Matter **82**, 43 (1991).
[37] E. A. Kotomin, R. W. Grimes, Y. Mastrikov, and N. J. Ashley, J. Phys.: Condens. Matter **19**, 106208 (2007).
[38] FPLO-5.00-18, improved version of the original FPLO code by K. Koepernik and H. Eschrig, Phys. Rev. B **59**, 1743 (1999); http://www.FPLO.de
[39] J. P. Moore, W. Fulkerson, and D. L. McElroy, J. Am. Ceram. Soc. **53**, 76 (1970).
[40] T. Ohmichi, T. Kikuschi, and S. Nasu, J. Nucl. Sci. Technol. **9**, 77 (1972).
[41] L. G. Radosevich and W. S. Williams, J. Am. Ceram. Soc. **52**, 514 (1969).
[42] W. Fulkerson, T. G. Kollie, S. C. Weaver, J. P. Moore, and R. K. Williams, *Proceedings of the Fourth International Conference on Plutonium and other Actinides* (AIME, Santa Fe, 1970), p. 374.
[43] E. Talik, M-E. Lucas, W. Suski, and R. Troć, J. Alloys Compd. **350**, 72 (2003).
[44] C. Sułkowski, T. Plackowski, and W. Sadowski, Phys. Rev. B **57**, 1231 (1998).
[45] A. Jeżowski, J. Mucha, and G. Pompe, J. Phys. D **20**, 1500 (1987).
[46] J. P. Perdew and Y. Wang, Phys. Rev. B **45**, 13244 (1992).
[47] J. J. Yeh and I. Lindau, At. Data Nucl. Data Tables **32**, 1 (1985).
[48] Q. G. Sheng and B. R. Cooper, J. Magn. Magn. Mater. **164**, 335 (1996).
[49] J. O. Scarbrough, H. L. Davis, W. Fulkerson, and J. O. Betterton, Jr., Phys. Rev. **176**, 666 (1968).
[50] S. Tougaard, J. Electron Spectrosc. Relat. Phenom. **52**, 243 (1990).
[51] S. Doniach and M. Šunjić, J. Phys. C **3**, 285 (1970).
[52] H. Grohs, H. Höchst, P. Steiner, S. Hüfner, and K. H. J. Buschow, Solid State Commun. **33**, 573 (1980).
[53] G. A. Slack, J. Appl. Phys. **31**, 1571 (1960).
[54] R. Kubo, Phys. Rev. **87**, 568 (1952); T. Nagamiya, J. Phys. Radium **20**, 70 (1959).
[55] R. Troć, J. Solid State Chem. **13**, 14 (1975).
[56] C. H. de Novion and P. Costa, J. Phys. (Paris) **33**, 257 (1972).
[57] M. Nakashima, Y. Haga, E. Yamamoto, Y. Tokiwa, M. Hedo, Y. Uwatoko, R. Settai, and Y. Onuki, J. Phys.: Condens. Matter **15**, S2007 (2003).
[58] N. Hessel Andersen and H. Smith, Phys. Rev. B **19**, 384 (1979).
[59] T. T. M. Palstra, A. A. Menovsky, and J. A. Mydosh, Phys. Rev. B **33**, 6527 (1986).
[60] A. B. Anskern and S. Aronson, J. Phys. Chem. Solids **28**, 1069 (1967).
[61] R. P. Pinto, M. M. Amado, M. E. Braga, and J. B. Sousa, J. Appl. Phys. **79**, 6355 (1996).
[62] G. P. Srivestava, in *The Physics of Phonons*, edited by A. Hilger (Bristol, New York, 1990).
[63] M. Kamimoto, Y. Takahashi, and T. Mukaibo, J. Nucl. Mater. **59**, 149 (1976).
[64] M. Hiroi, M. Sera, N. Kobayashi, Y. Haga, E. Yamamoto, and Y. Onuki, J. Phys. Soc. Jpn. **66**, 1595 (1997).
[65] B. R. Cooper, Q. G. Sheng, U. Benedit, and P. Link, J. Alloys Compd. **213/214**, 120 (1994).
[66] W.-D. Schneider and C. Laubschat, Phys. Rev. Lett. **46**, 1023 (1981).
[67] G. Chełkowska, J. A. Morkowski, A. Szajek, J. Stępień-Damm, and R. Troć, Eur. Phys. J. B **35**, 349 (2003); A. Szytuła, A. Jezierski, A. Winiarski, B. Penc, and V. H. Tran, J. Phys.: Condens. Matter **18**, 4355 (2006).
[68] R. Troć, J. Alloys Compd. **442**, 34 (2007), and references therein.
[69] A. Le. R. Dawson, W. R. Datars, J. D. Garsett, and F. S. Razavi, J. Phys.: Condens. Matter **1**, 6817 (1989).
[70] Y. Tokiwa, Y. Haga, E. Yamamoto, D. Aoki, W. Watanabe, R. Settai, T. Inone, K. Kindo, H. Harima, and Y. Onuki, J. Phys. Soc. Jpn. **70**, 1744 (2001).
[71] D. Kaczorowski, R. Troć, D. Badurski, A. Böhm, L. Shlyk, and F. Steglich, Phys. Rev. B **48**, 16425 (1993).
[72] J. M. Robinson, Phys. Rep. **51**, 1 (1979); P. Erdös and J. M. Robinson, *The Physics of Actinide Compounds* (Plenum, New York, 1983).
[73] T. Takahashi, N. Sato, T. Yokoya, A. Chainani, T. Morimoto, and T. Komatsubara, J. Phys. Soc. Jpn. **65**, 156 (1996).
[74] Y. B. Ning, J. D. Garrett, C. V. Stager, and W. R. Datars, Phys. Rev. B **46**, 8201 (1992).
[75] R. H. Lemmer and J. E. Lowther, J. Phys. C **11**, 1145 (1978).
[76] Ch.-H. De Novion, C. R. Acad. Sci. Paris Serie **273**, 26 (1971).
[77] J. Grunzweig-Genossar, Solid State Commun. **8**, 1673 (1970).
[78] H. Kawanaka, H. Nakotte, E. Brück, K. Prokeš, N. H. Kim-Ngan, T. Takabatakes, H. Fujii, and J. Sakurai, Physica B **237-238**, 226 (1997).
[79] K. Mortensen, Solid State Commun. **44**, 643 (1982).
[80] J. B. Sousa, R. S. Pinto, M. M. Amado, J. M. Moreira, M. E. Braga, M. Ausloos, and I. Balberg, Solid State Commun. **31**, 209 (1979).

[81] S. B. Palmer and E. W. Lee, Phil. Mag. **24**, 311 (1971); K. W. Katahara, M. Nimalendrain, M. H. Manghanani, and E. S. Fisher, J. Phys. F: Met. Phys. **9**, 2167 (1979).
[82] F. Honda, N. Metoki, T. D. Matsuda, Y. Haga, and Y. Onuki, J. Phys.: Condens. Matter **18**, 479 (2006).
[83] A. K. Bhattacharjee and B. Coqblin, Phys. Rev. B **38**, 338 (1988).
[84] D. Kaczorowski, R. Troć, and H. Noël, J. Phys.: Condens. Matter **3**, 4959 (1991).
[85] A. Krimmel, A. Loidl, R. Eccleston, C. Geibel, and F. Steglich, J. Phys.: Condens. Matter **8**, 1677 (1996).
[86] M. Marutzky, U. Barkow, J. Schoenes, and R. Troć, J. Magn. Magn. Mater. **299**, 225 (2006).